Graphene Oxide Enhances Cellular Delivery of Hydrophilic Small Molecules by Co-Incubation
Supporting Information

Andy H. Hung,[†] Robert J. Holbrook,[†] Matthew W. Rotz,[†] Cameron J. Glasscock,[†] Nikhita D. Mansukhani,[‡] Keith W. MacRenaris,[†] Lisa M. Manus,[†] Matthew C. Duch,[‡] Kevin T. Dam,[†] Mark C. Hersam,[*,‡] and Thomas J. Meade[*,†]

[†]Department of Chemistry, Molecular Biosciences, Neurobiology, Biomedical Engineering, and Radiology, Northwestern University, 2145 Sheridan Road, Evanston, Illinois 60208-3113, United States

[‡]Department of Materials Science and Engineering and Department of Chemistry, Northwestern University, 2220 Campus Drive, Evanston, Illinois 60208-3108, United States

Table of Contents

1. Supplementary Materials and Methods

1.1. Synthesis of Gd(III)-labeled Molecules

Tris-Hydroxypropyl Triazolyl Amine (THPTA) and Tris-Benzyl Triazolyl Amine (TBTA) used as stabilizing and solubilizing ligands for copper(I) during click reactions were synthesized and purified according to literature procedure.[1,2] Gd(HPN$_3$DO3A) used in the synthesis of **1**-**7** was synthesized using previously published procedures.[3] 1,4,7-(Tris-*tert*-butyl acetate)-1,4,7,10-tetraazacyclodecane·HBr (*tert*-butyl DO3A) used in the synthesis of **8**-**11** was synthesized as previously described.[4]

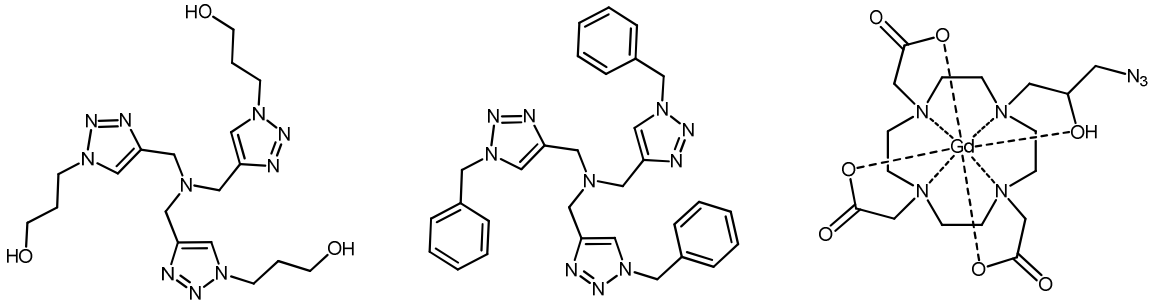

The HPLC mobile phases consisted of deionized water (Solvent A) and HPLC-grade acetonitrile (Solvent B). Where applicable, a Waters 4.6 x 150 mm X-Bridge analytical C18 5 µm column and the semi-preparative equivalent, 19 x 150 mm were used. Solvents used with this column consisted of aqueous ammonium hydroxide, pH = 10.37 (Solvent C) and HPLC-grade acetonitrile (Solvent D).

1.1.1. Synthesis of **1**

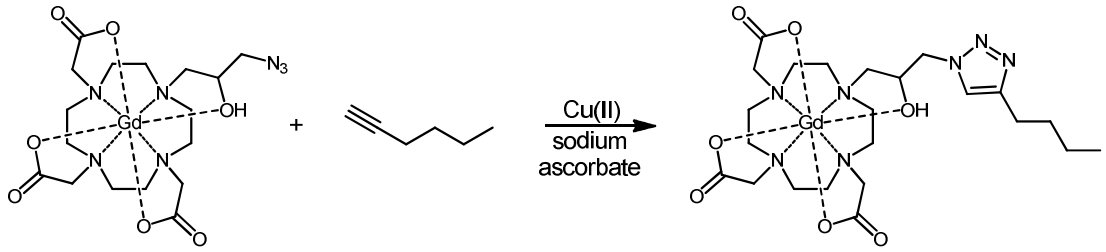

To a 250 mL round bottom flask was added water (25 mL), [Gd(HPN$_3$DO3A)(H$_2$O)] (0.150 g, 0.25 mmol) and Cu(II)SO$_4$ · 5 H$_2$O (0.006 g, 0.025 mmol). To the stirring mixture was added tetrahydrofuran (24 mL). To a 2 mL glass vial was added tetrahydrofuran (1 mL), 1-hexyne (0.041 g, 0.50 mmol), and tris-benzyltriazolylamine (0.016 g, 0.03 mmol). The tetrahydrofuran containing the dissolved 1-hexyne and TBTA was then added to the stirring mixture of [Gd(HPN$_3$DO3A)(H$_2$O)] and Cu(II)SO$_4$ · 5 H$_2$O. To this was added sodium ascorbate (0.05 g, 0.25 mmol) and the mixture was left to stir under nitrogen overnight at room temperature. The crude mixture was purified by semipreparative reverse phase HPLC using the following conditions: 0-5 min 0 % solvent B, 20 min 40 % solvent B, 25 min 100% solvent B, 25-30 min 0 % solvent B, 35 min 0% Solvent B and 35-40 min 0 % solvent B. The desired product elutes from 20.6 to

21.8 minutes as monitored by UV-vis at 201/210 nm and was collected and lyophilized. Yield: 0.121 g (71 %). (*m/*z): observed: 681.3, calculated: 681.8 $[M + H]^+$.

1.1.2. Synthesis of **2**

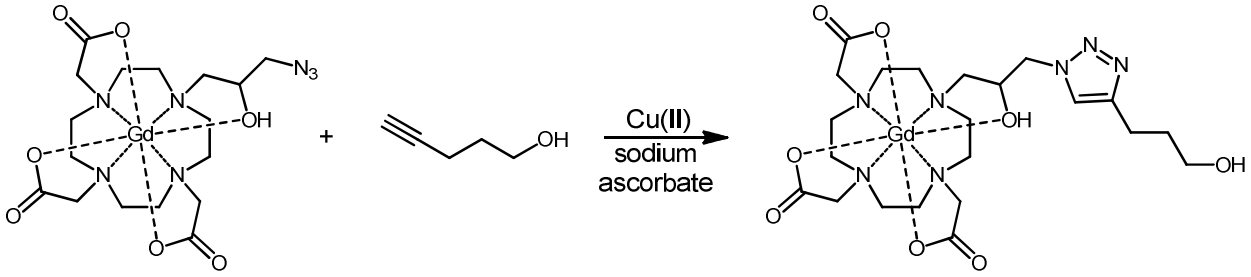

To a 250 mL round bottom flask was added water (75 mL) and [Gd(HPN_3DO3A)(H_2O)] (0.150 g, 0.25 mmol), Cu(II)SO_4 · 5 H_2O (0.006 g, 0.025 mmol) and tris-hydroxypropyltriazolylamine (0.013 g, 0.03 mmol). With dissolution of these components was then added *tert*-butanol (24 mL). To a separate, 2 mL glass vial was added *tert*-butanol (1 mL) and 4-pentyne-1-ol (0.042 g, 0.50 mmol). To the stirring solution of [Gd(HPN_3DO3A)(H_2O)], Cu(II) and THPTA was added the solution of 4-pentyn-1-ol in *tert*-butanol. To this was further added sodium ascorbate (0.05 g, 0.25 mmol) and the mixture was left to stir under nitrogen overnight at room temperature. The crude mixture was purified by semipreparative reverse phase HPLC using the following conditions: 0-5 min 0 % solvent B, 20 min 40 % solvent B, 25 min 100% solvent B, 25-30 min 0 % solvent B, 35 min 0% Solvent B and 35-40 min 0 % solvent B. The desired product elutes from 16.4 to 16.8 minutes as monitored by UV-vis at 201/210 nm and was collected and lyophilized. Yield: 0.125 g (73 %). (*m/*z): observed: 683.1, calculated: 683.8 $[M + H]^+$.

1.1.3. Synthesis of **3**

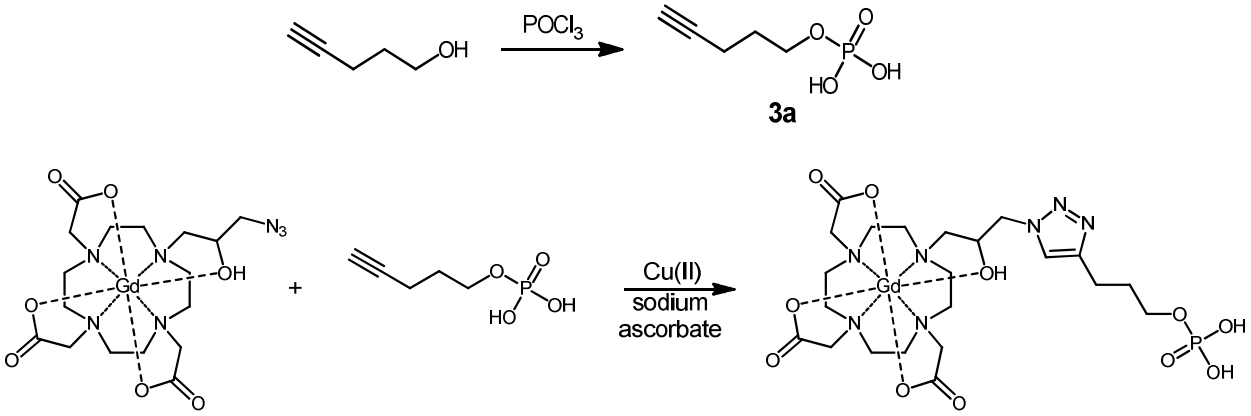

pent-4-yn-1-yl dihydrogen phosphate (3a): To an oven-dried 50 mL round bottom flask was added a magnetic stir bar and anhydrous diethyl ether (25 mL). To the stirring solvent was added 4-pentyne-1-ol (0.452 g, 6.57 mmol), triethylamine (0.665 g, 6.57 mmol), and pyridine (1.039 g, 13.14 mmol). To a second, oven-dried 100 mL round bottom flask was added anhydrous diethyl ether (25 mL) and phosphorous oxychloride (1.211 g, 7.90 mmol). The flask containing phosphorous oxychloride was cooled to 0 °C with stirring, at which time was added dropwise the solution of 4-pentyne-1-ol over two

hours, whereupon the mixture became cloudy with a visible white suspension. After the complete addition of 4-pentyne-1-ol solution, the reaction mixture was allowed to warm to room temperature and remain stirring for a further 12 hours. The pale brown mixture was then cooled again to 0 °C open to the atmosphere, and water (5 mL) was added and the reaction left to stir for one hour. To the stirring biphasic mixture was added 10 mL of 1M NaOH (aq), followed by separation of the organic phase using a separatory funnel and further extraction of the aqueous layer using additional diethyl ether (2 x 10 mL). To the isolated aqueous mixture was then added 15 mL of 1M HCl (aq), followed by extraction with ethyl acetate (3 x 10 mL). Successful synthesis and isolation of the product in the ethyl acetate was confirmed by ESI-MS of the phosphorylated product (*m/*z): observed: 162.8, calculated: 163.1 $[M - H]^-$. The crude product was taken forward without further purification.

Gd(HPN$_3$DO3A)-phosphate (3): To a 250 mL round bottom flask was added 0.5 M triethylammonium acetate buffer pH 7.0 (100 mL), [Gd(HPN$_3$DO3A)(H$_2$O)] (0.150 g, 0.25 mmol), Cu(II)SO$_4$ · 5 H$_2$O (0.006 g, 0.025 mmol), tris-hydroxypropyltriazolylamine (0.013 g, 0.03 mmol), and **3a** (unpurified, approximately 6.0 mmol). To this was further added sodium ascorbate (0.05 g, 0.25 mmol) and the mixture was left to stir overnight under nitrogen at room temperature. The crude mixture was purified by semipreparative reverse phase HPLC using the following conditions: 0-5 min 0 % solvent B, 20 min 40 % solvent B, 25 min 100% solvent B, 25-30 min 0 % solvent B, 35 min 0% Solvent B and 35-40 min 0 % solvent B. The desired product elutes from 10.4 to 12.5 minutes as monitored by UV-vis at 201/210 nm and was collected and lyophilized. Yield: 0.095 g (54 %). (*m/*z): observed: 763.3, calculated: 763.8 $[M + H]^+$

1.1.4. Synthesis of **4**

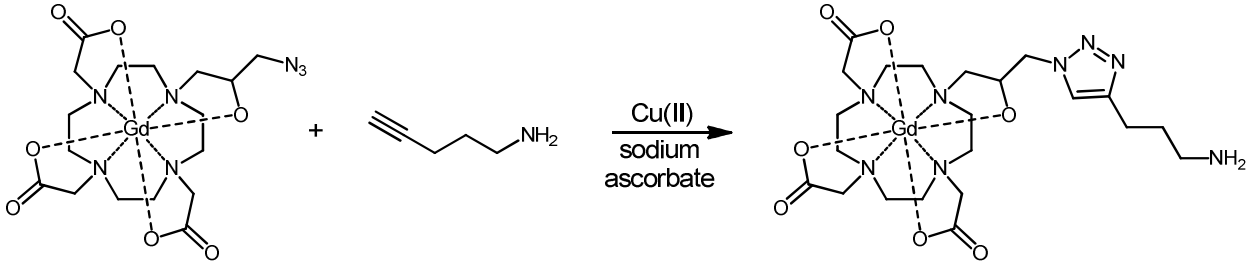

To a 250 mL round bottom flask was added water (12.5 mL), [Gd(HPN$_3$DO3A)(H$_2$O)] (0.05 g, 0.083 mmol) and then 12.5 mL 1,4-Dioxane. Cu(II)SO$_4$ · 5 H$_2$O (0.003 g, 0.0125 mmol) was then added to the stirring mixture. To a 2 mL glass vial was added 1,4-Dioxane (1 mL), 4-pentyne-1-amine (0.021 g, 0.25 mmol). The 1,4-Dioxane containing the dissolved 4-pentyne-1-amine was then added to the stirring mixture of [Gd(HPN$_3$DO3A)(H$_2$O)] and Cu(II)SO$_4$ · 5 H$_2$O. To this was added sodium ascorbate (0.05 g, 0.25 mmol) and the mixture was left to stir under nitrogen overnight at room temperature. The crude mixture was purified by semipreparative reverse phase HPLC using the following conditions: 0-15 min 0 % solvent B, 22 min 10 % solvent B, 30 min 100% solvent B, 30-35 min 0 % solvent B, 40 min 0% Solvent B and 40-45 min 0 % solvent B. The desired product elutes from 25.2 to 25.6 minutes as monitored by UV-vis at 201/210 nm and was collected and lyophilized. Yield: 0.023 g (40.9 %). (*m/*z): observed: 684.1, calculated: 683.2 $[M + H]^+$.

1.1.5. Synthesis of **5**

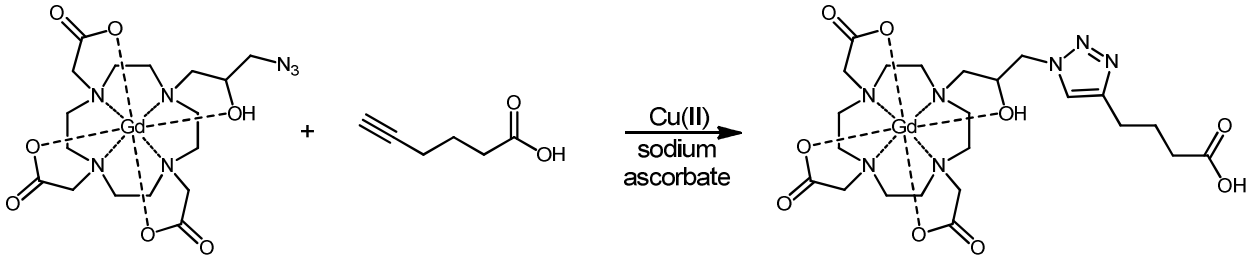

To a 250 mL round bottom flask was added water (100 mL) and [Gd(HPN$_3$DO3A)(H$_2$O)] (0.150 g, 0.25 mmol), Cu(II)SO$_4$ · 5 H$_2$O (0.006 g, 0.025 mmol), tris-hydroxypropyltriazolylamine (0.013 g, 0.03 mmol) and 5-hexynoic acid (0.056 g, 0.50 mmol). To this was further added sodium ascorbate (0.05 g, 0.25 mmol) and the mixture was left to stir under nitrogen overnight at room temperature. The crude mixture was purified by semipreparative reverse phase HPLC using the following conditions: 0-5 min 0 % solvent B, 20 min 40 % solvent B, 25 min 100% solvent B, 25-30 min 0 % solvent B, 35 min 0% Solvent B and 35-40 min 0 % solvent B. The desired product elutes from 10.2 to 11.3 minutes as monitored by UV-vis at 201/210 nm and was collected and lyophilized. Yield: 0.095 g (54 %). (*m/*z): observed: 711.1, calculated: 711.8 $[M + H]^+$.

1.1.6. Synthesis of **6**

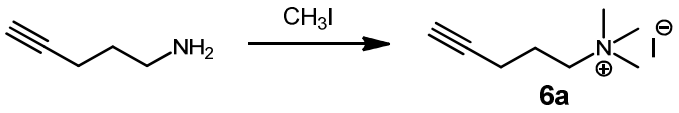

6a

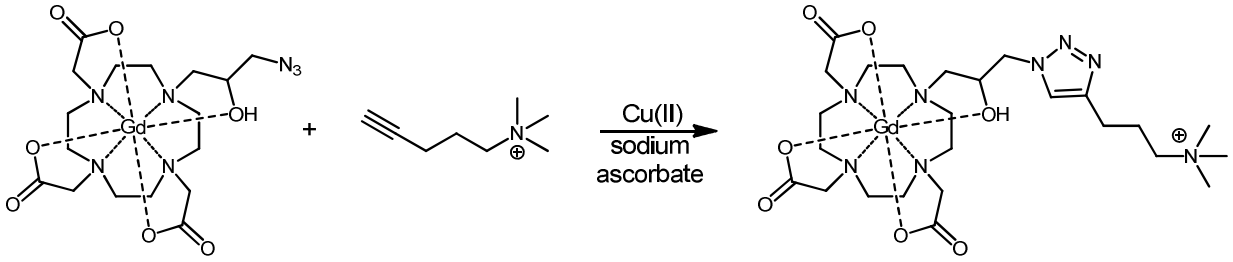

N,N,N-trimethylpent-4-yn-1-ammonium Iodide (6a): To a dried 10 mL round bottom flask was added a magnetic stir bar, and anhydrous acetonitrile (5 mL). Potassium carbonate (0.500 g, 3.6 mmol) and 4-pentyn-1-amine (0.075 g, 0.90 mmol) were further added. To the stirring mixture containing some visible, insoluble potassium carbonate was added methyl iodide (0.460 g, 3.24 mmol). The reaction was stirred for 12 hours at room temperature. After such time, the reaction was filtered, and evaporated yielding a mixture of the pale yellow solid of the tetra-alkyl iodide product and potassium carbonate. Full conversion of starting material to product was confirmed by ESI-MS. (*m/*z): observed: 126.4, calculated: 126.2 $[M]^+$. The solid, crude product was taken forward without further purification.

Gd(HPN$_3$DO3A)-tertiary amine (6): To a 250 mL round bottom flask was added water (75 mL) and [Gd(HPN$_3$DO3A)(H$_2$O)] (0.150 g, 0.25 mmol), Cu(II)SO$_4$ · 5 H$_2$O (0.006 g, 0.025 mmol) and tris-

hydroxypropyltriazolylamine (0.013 g, 0.03 mmol). After dissolution of these components was then added *tert*-butanol (25 mL). To a separate, 2 mL glass vial was added 1:1 *tert*-butanol:water (1 mL) and compound **6a** (unpurified, approximately 0.9 mmol). To the stirring solution of [Gd(HPN$_3$DO3A)(H$_2$O)], Cu(II) and THPTA was added the solution of 4-pentyn-1-ol in the *tert*-butanol water mixture. To this was further added sodium ascorbate (0.05 g, 0.25 mmol) and the mixture was left to stir under nitrogen overnight at room temperature. The crude mixture was purified by semipreparative reverse phase HPLC using the following conditions and solvents C and D: 0-5 min 5 % solvent C, 20 min 40 % solvent C, 25 min 100% solvent C, 25-30 min 0 % solvent C, 35 min 0% Solvent C and 35-40 min 5 % solvent C. The desired product elutes from 4.7 to 6.3 minutes as monitored by UV-vis at 201/210 nm and was collected and lyophilized. Yield: 0.125 g (73 %). (*m/*z): observed: 725.0, calculated: 724.9 $[M + H]^+$.

1.1.7. Synthesis of **7**

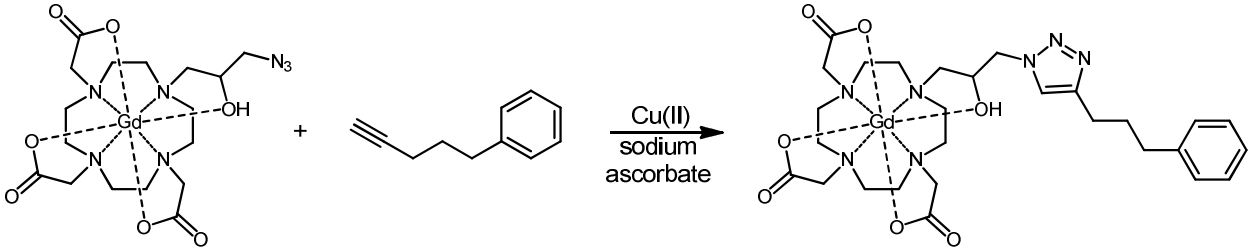

To a 250 mL round bottom flask was added water (25 mL), [Gd(HPN$_3$DO3A)(H$_2$O)] (0.150 g, 0.25 mmol) and Cu(II)SO$_4$ · 5 H$_2$O (0.006 g, 0.025 mmol). To the stirring mixture was added tetrahydrofuran (24 mL). To a 2 mL glass vial was added tetrahydrofuran (1 mL), 5-phenyl-1-pentyne (0.072 g, 0.50 mmol), and tris-hydroxybenzyltriazolylamine (0.016 g, 0.03 mmol). The tetrahydrofuran containing the dissolved 5-phenyl-1-pentyne and TBTA was then added to the stirring mixture of [Gd(HPN$_3$DO3A)(H$_2$O)] and Cu(II)SO$_4$ · 5 H$_2$O. To this was added sodium ascorbate (0.05 g, 0.25 mmol) and the mixture was left to stir under nitrogen overnight at room temperature. The crude mixture was purified by semipreparative reverse phase HPLC using the following conditions: 0-5 min 0 % solvent B, 20 min 40 % solvent B, 25 min 100% solvent B, 25-30 min 0 % solvent B, 35 min 0% Solvent B and 35-40 min 0 % solvent B. The desired product elutes from 25.4 to 26.4 minutes as monitored by UV-vis at 201/210 nm and was collected and lyophilized. Yield: 0.156 g (84 %). (*m/*z): observed: 742.4, calculated: 743.9 $[M + H]^+$.

1.1.8. Synthesis of **8**

DO3A-tris-tert-butyl ester·HBr was synthesized according to previously published procedures.[4] An aqueous trifluoroacetic acid (TFA) solution, 30:1:1 (TFA:triethylsilane:H$_2$O) was added and stirred at room temperature overnight to deprotect the ligand. TFA was removed from the solution by purging with a stream of nitrogen and concentrating from water twice. 1 equivalent of Gd(CH$_2$COO)$_3$·xH$_2$O was added and the pH of the solution adjusted with 1M NaOH and 1M HCl to 6.5. The resultant was stirred at 60 °C overnight. The crude mixture was purified by semipreparative reverse phase HPLC.

1.1.9. Synthesis of **9**

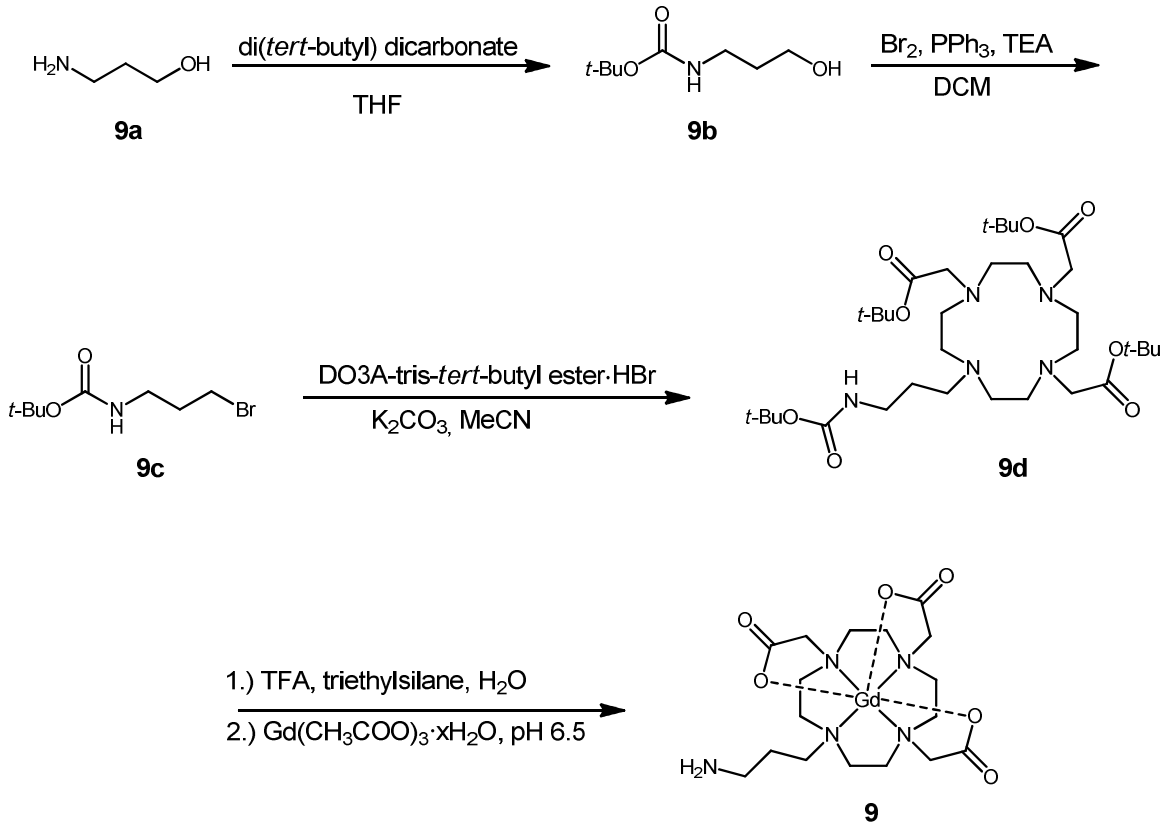

***N*-(*tert*-butoxycarbonyl)-3-hydroxypropylamine (9b):** Di-*tert*-butyl dicarbonate (3.046 g, 13.9 mmol) was dissolved in 50 mL of tetrahydrofuran (THF). 3-amino propanol (**9a**, 1.062 mL, 13.9 mmol) suspended in 50 mL of THF was then added and the reaction stirred at room temperature overnight. The reaction mixture was concentrated under reduced pressure and the crude material purified by flash column chromatography over silica gel with 1:9 methanol:dichloromethane (MeOH:DCM) to afford a pale yellow oil (2.425 g, 99%). ^{1}H NMR (500 MHz, $CDCl_3$): δ 4.86 (bs, 1H), 3.66 (m, 2H), 3.29 (quar, 2H, *J* = 6.4, 6.0), 3.19 (bs, 1H), 1.67 (quin, 2H, *J* = 6.0), 1.45 (s, 9H). ^{13}C NMR (126 MHz, $CDCl_3$): 157.26, 79.71, 59.14, 36.82, 32.87, 28.36.

***N*-(*tert*-butoxycarbonyl)-3-bromopropylamine (9c):** Triphenylphosphine (1.553 g, 5.9 mmol) was dissolved in 30 mL of dichloromethane and cooled to 0 °C. triethylamine (0.830 mL, 5.9 mmol) was added via syringe. Bromine (0.305 mL, 5.9 mmol) diluted in 20 mL of DCM was added via syringe and the reaction vessel stirred at 0 °C for 1 hr. Upon warming to room temperature, **9b** (0.852 g, 5.4 mmol) suspended in 10 mL of DCM was added via syringe. The reaction mixture was stirred at room temperature overnight. Upon concentration under reduced pressure, the crude reaction was purified by flash column chromatography over silica gel with 1:5 ethyl acetate/hexanes (EtOAc:Hex) to give a yellow oil (0.713 g, 3.2 mmol, 60%). ^{1}H NMR (500 MHz, $CDCl_3$): δ 4.69 (bs, 1H), 3.45 (t, 2H), 3.27 (quar, 2H), 2.06 (quin, 2H), 1.44 (s, 9H) ^{13}C NMR (126 MHz, $CDCl_3$): δ 155.97, 79.47, 38.96, 32.65, 30.89, 28.40.

tri-tert-butyl 2,2',2''-(10-(3-((tert-butoxycarbonyl)amino)propyl)-1,4,7,10-tetraazacyclododecane-1,4,7-triyl)triacetate (9d): DO3A-tris-tert-butyl ester·HBr was synthesized according to previously published procedures.[4] DO3A-tris-tert-butyl ester·HBr (2.731 g, 4.6 mmol) and **9c** (1.150 g, 4.8 mmol) were dissolved in 50 mL of MeCN. Anhydrous potassium carbonate (1.614 g, 11.7 mmol) was added and the reaction stirred overnight at 60 °C. Reaction progress was monitored by mass spectrometry. The crude material was filtered, concentrated under reduced pressure, and purified by flash chromatography over silica gel using 1:9 MeOH:DCM (Pt stain) to give the product as an oily solid (2.526 g, 3.4 mmol, 82%). ^{1}H NMR (500 MHz, $CDCl_3$): δ 3.64-2.29 (m, 22H), 1.65 (bs, 4H), 1.48-1.43 (m, 36H). ^{13}C NMR (500 MHz, $CDCl_3$): δ 172.70, 155.96, 82.63, 82.28, 55.77, 51.77, 38.82, 37.86, 28.44, 28.01, 27.81, 26.84. ESI-MS (*m/*z): Calcd. for $[M + H]^+$: 671.5 Found: 671.8.

gadolinium(III)2,2',2''-(10-(3-(amino)propyl)-1,4,7,10-tetraazacyclododecane-1,4,7-tryl)triacetate (9): An aqueous trifluoroacetic acid (TFA) solution, 30:1:1 (TFA:triethylsilane:H_2O) was added to **9d** (0.241 g, 0.4 mmol) at room temperature. The resultant was stirred at room temperature overnight. Complete deprotection was observed after 18 hours. TFA was removed from the solution by purging with a stream of nitrogen and concentrating from water twice. Upon resuspension in 20 mL H_2O, Gd(III) acetate hydrate [$Gd(CH_3CO)_3$·xH2O, 0.118 g, 0.4 mmol) was added and the pH of the solution adjusted with 1M NaOH and 1M HCl to 6.5. The resultant was stirred at 60 °C overnight. The crude mixture was purified by semipreperative HPLC on a reverse phase C18 column, eluting using the following method: initial conditions of 0% B were held constant for 6 min, ramp to 12% B over 3 min, wash at 100 % B for 5 min followed by return to 0% B. The product fractions (8.43-11.00 min by UV/vis at 200 nm and 210 nm) were collected and freeze-dried (0.122 g, 0.2 mmol 62 %). Analytical LC-MS showed a single peak with *m/z* = 558.6; ($[M + H]^+$).

1.1.10. Synthesis of **10**

10 was synthesized following previously published procedures.[5] ESI-MS (m/z) observed: 601.1990, calculated: 601.1979 $[M + H]^+$. Elemental Analysis calculated for Na[C20H36GdN5O6]·H2O·TFA: C, 35.01; H, 5.21; N, 9.28. Found: C, 35.16; H, 5.39; N, 9.16.

1.1.11. Synthesis of **11:**

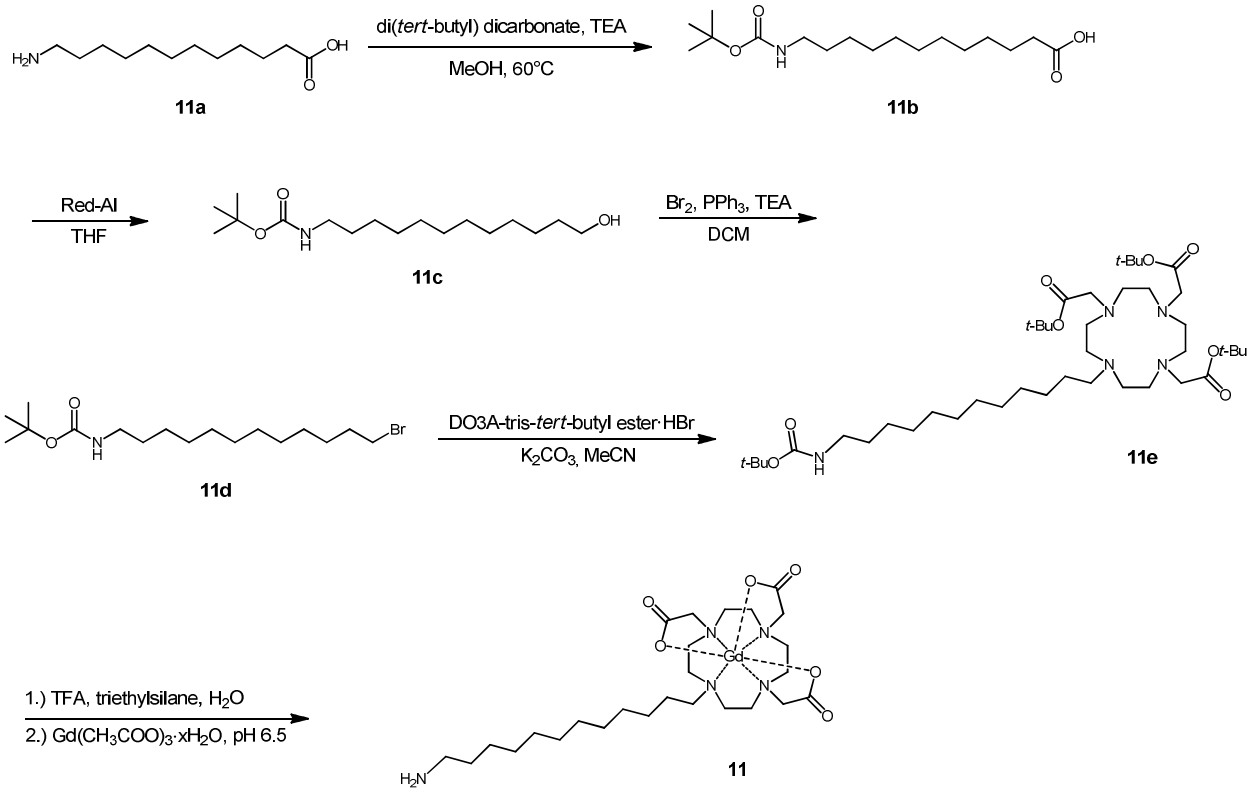

12-(*N*-*tert*-butoxycarbonyl)aminododecanoic acid (11b): 12-aminododeconic acid (**11a**, 1.066 g, 5.0 mmol), triethylamine (0.800 mL, 5.7 mmol), and boc anhydride (1.053 g, 4.8 mmol) were combined in 15 mL of MeOH and refluxed at 60 °C overnight. The reaction mixture was removed from heat and concentrated under reduced pressure. The resultant residue was redissolved in ethyl acetate, washed with 0.25 M HCl, dried over MgSO4, filtered, and concentrated. The desired colorless, crystalline solid was obtained by recrystallizaton with hexanes (1.250 g, 4.0 mmol, 80 %). ^{1}H NMR (500 MHz, $CDCl_3$): δ 4.54 (bs, 1H), 3.11 (2H, quar), 2.35 (t, 2H), 1.63 (quin, 2H), 1.45 (s, 11H), 1.27 (m, 14H). ^{13}C NMR (126 MHz, $CDCl_3$): δ 179.08, 155.04, 79.11, 41.75, 40.64, 33.97, 30.03, 29.41, 29.33, 29.25, 29.17, 29.01, 28.44, 26.79, 24.70.

***N*-(*tert*-butoxycarbonyl)-12-hydroxydodecylamine (11c):** Boc-lauric acid (**11b**, 1.005 g, 3.2 mmol) was dissolved in 25 mL of tetrahydrofuran. Red-Al [70% (w/w) in toluene, 2.7 mL, 9.5 mmol] was added dropwise via syringe over 10 minutes at room temperature. The reaction mixture was stirred for thirty minutes after the precipitant dissolved (approximately 2 hrs total). At this point, the reaction was quenched with a saturated solution of Na_2SO_4 (aq) followed by stirring for an additional 1 hour at room temperature. The resultant solution was concentrated under reduced pressure, resuspended in ethyl acetate, washed with water, dried over MgSO4, filtered, and concentrated. Recrystallizaton with toluene afforded a crystalline, colorless solid (0.663 g, 2.2 mmol, 86%). ^{1}H NMR (500 MHz, $CDCl_3$): δ 4.54 (bs, 1H), 3.66 (t, 2H), 3.12 (quar, 2H), 1.68 (bs, 1H), 1.59 (quin, 2H), 1.46 (s, 11H), 1.29 (m, 16H). ^{13}C NMR (126 MHz, $CDCl_3$): δ 156.01, 79.04, 63.09, 40.63, 32.81, 30.07, 29.58, 29.42, 29.29, 28.45, 26.81, 25.73.

***N*-(*tert*-butoxycarbonyl)-12-bromododecylamine (11d):** Triphenylphosphine (0.488 g, 1.9 mmol) was dissolved in 10 mL of dichloromethane and cooled to 0 °C. Triethylamine (0.260 mL, 1.9 mmol) was added via syringe. Bromine (0.100 mL, 1.9 mmol) diluted in 15 mL of DCM was then added via syringe and the reaction vessel maintained at 0 °C for 1 hour. Upon warming to room temperature, **11c** (0.5067 g, 1.7 mmol) in 6 mL of DCM was added and the reaction vessel stirred at room temperature overnight. Reaction progress was monitored by thin layer chromatography. The reaction volume was concentrated under reduced pressure followed by flash column chromatography purification of the crude material with ethyl acetate:hexanes (5:1) to give a colorless, crystalline solid (0.411 g, 1.1 mmol, 67%). Alternatively, the pure material can be obtained from recrystallizaton with acetonitrile. ^{1}H NMR (500 MHz, $CDCl_3$): δ 4.61 (bs, 1H), 3.41 (t, 2H), 3.10 (quar, 2H), 1.85 (quin, 2H), 1.44 (m, 12H), 1.27 (m, 15H). ^{13}C NMR (126 MHz, $CDCl_3$): δ 155.97, 78.91, 40.62, 34.04, 32.82, 30.05, 29.52, 29.50, 29.41, 29.28, 28.75, 28.42, 28.16, 26.80.

tri-*tert*-butyl 2,2',2''-(10-(12-(tert-butoxycarbonylamino)dodecyl)-1,4,7,10-tetraazacyclododecane-1,4,7-triyl)triacetate (11e): Tris-tert-butyl DO3A·HBr (0.213 g, 0.4 mmol) and **11d** (0.132 g, 0.4 mmol) were combined in acetonitrile (10 mL). Anhydrous potassium carbonate (0.126 g, 0.92 mmol) was added. The reaction was stirred at 60 ºC for sixteen hours then cooled to room temperature and filtered rinsing with acetonitrile. The crude material was purified by flash column chromatography eluting with 1:9 methanol:dicholoromethane (detected with Pt stain) and fractions concentrated to give a yellow oily solid (0.257 g, 0.3 mmol, 90%). ^{1}H NMR (500 MHz, d_6-DMSO): δ 3.42-2.62 (m, 17 H), 2.37-2.06 (m, 5H), 1.45-1.22 (m, 53H). ^{13}C NMR (126 MHz, DMSO): δ 173.22, 172.59, 170.25, 166.93, 155.50, 131.57, 128.62, 81.64, 81.50, 80.55, 77.20, 67.32, 65.66, 55.85, 55.31, 53.89, 51.81, 49.82, 48.55, 38.02, 33.19, 26.21, 25.51, 23.91, 23.19, 22.38, 13.88, 10.78. ESI-MS (*m/*z): Calcd. for $[M + H]^+$: 797.6 Found: 798.7.

Gadolinium(III) 2,2',2''-(10-(12-(amino)dodecyl)-1,4,7,10-tetraazacyclododecane-1,4,7-tryl)triacetate (11): An aqueous TFA solution, 30:1:1 (TFA:triethylsilane:H2O) was added to **11e** (0.238 g, 0.3 mmol) at room temperature. The resultant was stirred at room temperature overnight. Deprotection was observed after 24 hours. TFA was removed from the solution by purging with a stream of nitrogen and concentrating from water twice. Upon resuspension in 20 mL H2O, $Gd(CH_2COO)_3 \cdot xH_2O$ (0.104 g, 0.3 mol) was added and the pH of the solution adjusted with 1M NaOH and 1M HCl to 6.5. The resultant was stirred at room temperature until pH was maintained at 6.5. The crude mixture was purified by semipreperative HPLC on a reverse phase C8 Sunfire column, eluting using the following method: : initial conditions of 5% B were held constant for 5 min, then a ramp to 100% B over 20 min, a wash at 100 % B for 4 min followed by return to 5% B. The product fractions (11:45-16:45 mins by UV/vis at 200 nm and 220 nm) were collected and freeze-dried (0.055 g, 0.08 mmol, 27%). Analytical LC-MS showed a single peak with *m/z* = 684.2 ($[M + H]^+$).

1.1.12. Magnevist [Gd(DTPA)(H_2O)] (**12**)

Diethylenetriaminepentaacetic acid gadolinium(III) dihydrogen salt hydrate was purchased from Sigma-Aldrich (Catalogue number 381667) and used as supplied. To make up a solution, Milli-Q water was added and the pH was adjusted to 7 using 2.0M NaOH.

1.1.13. Synthesis of **13**

Magnevist-NH_2 (**13**) was synthesized following previously published procedures developed by our group.[6] ESI-MS (m/z) observed: 617.1, calculated: 617.1 $[M]^-$.

1.1.14. Synthesis of ProHance [Gd(HP-DO3A)(H_2O)] (**14**)

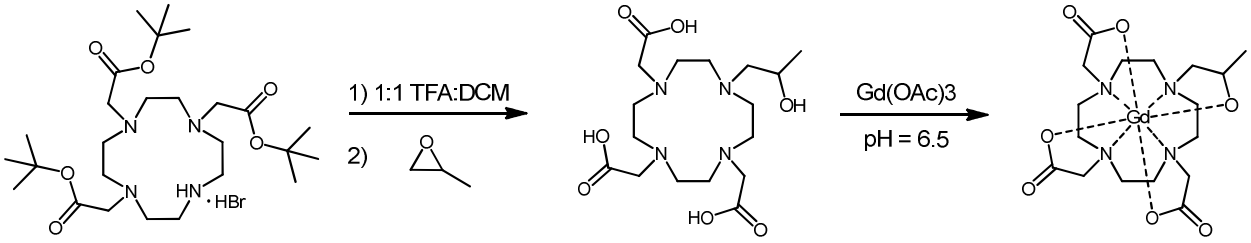

To a 100 mL round bottom flask charged with a magnetic stir bar and *tert*-butyl DO3A · HBr (0.278 g, 0.47 mmol) was added 1:1 trifluoroacetic acid and dichloromethane (25 mL). Upon addition of the solvent/acid mixture, the reaction turned a pale orange, transparent color and was left to stir for 12 hours at room temperature. After such time, all solvent was evaporated resulting in a pale brown oil. To verify complete deprotection, ESI-MS was used to observe the complete loss of starting material (product (*m/*z): observed: 346.1, calculated: 346.4 $[M + H]^+$). To the pale brown oil was added water (20 mL), and aqueous 1.25 M NaOH until the solution was pH = 12. To this stirring, basic mixture was added propylene oxide (0.081 g, 1.40 mmol). The reaction was then left to stir for 12 hours at room temperature. The complete reaction of DO3A was verified by ESI-MS (product (*m/*z): observed: 405.7, calculated: 405.5 $[M + H]^+$). The mixture was then acidified using aqueous 1M HCl until the solution was pH = 4. To the stirring, acidic mixture was added gadolinium(III) acetate hydrate (0.250 g, 0.75 mmol). The pH of the resulting solution was adjusted to pH = 6.5 and monitored until stable using 1.25 M aqueous NaOH. The reaction was then left to stir for a further 12 hours at room temperature. The crude mixture was purified by semipreparative reverse phase HPLC using the following conditions: 0-5 min 0 % solvent B, 20 min 40 % solvent B, 25 min 100% solvent B, 25-30 min 0 % solvent B, 35 min 0% Solvent B and 35-40 min 0 % solvent B. The desired product elutes from 15.9 to 16.6 minutes as monitored by UV-vis at 201/210 nm and was collected and lyophilized. Yield: 0.066g (25 %). (*m/*z): observed: 559.2, calculated: 559.7 $[M + H]^+$.

1.1.15. Synthesis of Dotarem [Gd(DOTA)(H_2O)] (**15**)

Unmetalated DOTA ligand was purchased from Macrocyclics, Inc., and was metalated using the same procedure as prior to generate **15**.[3]

1.2. Alternative Molecular Adsorption Assay

An alternative method of characterizing adsorption was investigated by measuring the amount of Gd remaining in supernatant after a single centrifugation at 14,800 RPM for 20 minutes. The difference in supernatant Gd concentration pre- and post-centrifugation was assumed to have been adsorbed to GO. Comparison showed a significant difference between the adsorption measured from the supernatant and the adsorption measured directly from the washed GO pellet (Figures 3a, S12). Direct measurement on the GO pellet was considered more accurate based on its predictive power for GO cell delivery enhancement.

2. Supplementary Figures

2.1. GO Characterization

All GO samples were characterized using atomic force microscopy (AFM), Raman spectroscopy, and X-ray photoelectron spectroscopy (XPS). AFM data for the 150 nm GO were reported previously,[7] while those for the 1500 nm GO are shown in Figure S1. The mean and median of the sizes measured are summarized in Table S1. The relatively consistent height of 0.85 nm across both the 150 nm GO and the 1500 nm GO indicates that these samples are predominantly single layer sheets.

Raman spectroscopy and XPS were used to probe the chemical structures of GO. Comparing the Raman spectra of the 1500 nm GO to the 150 nm GO, the larger sample showed an increase in the D band relative to the G band, and a broadening of the 2D and G+D band areas (Figure S2). This result is similar to that observed for GO after solvothermal reduction[8] and that of graphene nanoribbons of increasing width.[9] Furthermore, XPS showed that the ratio of carbon-carbon bonds (C-C) to carbon-oxygen bonds (C-O, C=O, C(O)O) increased with GO size. The fitted C-C : C-O : C=O : C(O)O distribution was 10 : 6.1 : 4.2 : 1.4 and 10 : 4.9 : 3.9 : 1.3 for the 150 nm and the 1500 nm GO, respectively (Figure S3). The Raman and XPS data together indicate that the smaller GO bears fewer vacancy defects and 10%-15% more oxygen groups compared to the larger GO. That the smaller GO has comparatively more carbon-oxygen bonds than the larger GO may be explained by its larger edge-to-surface ratio. The edges of GO produced by the modified Hummers method are thought to be generously decorated with oxygen-containing functional groups.[10,11]

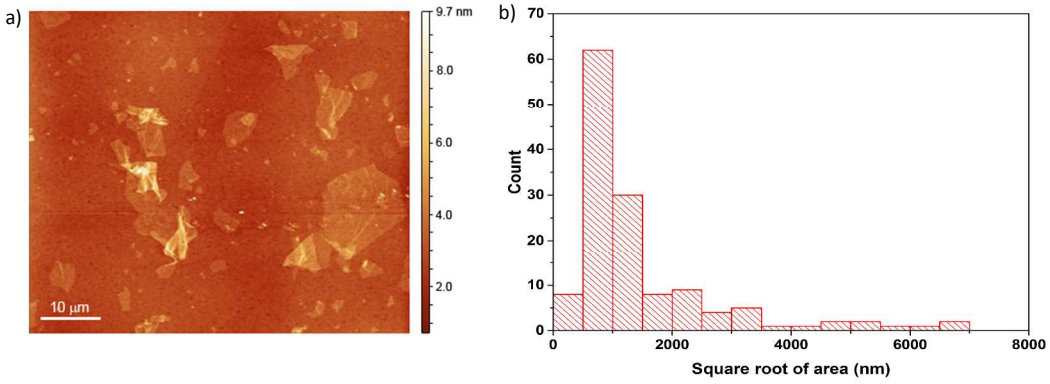

Figure S1. a) Representative atomic force microscopy image of the 1500 nm GO. b) Distribution of the GO lateral size as characterized by square root of area. GO sheets from at least 5 separate areas were counted for a total of more than 150 sheets.

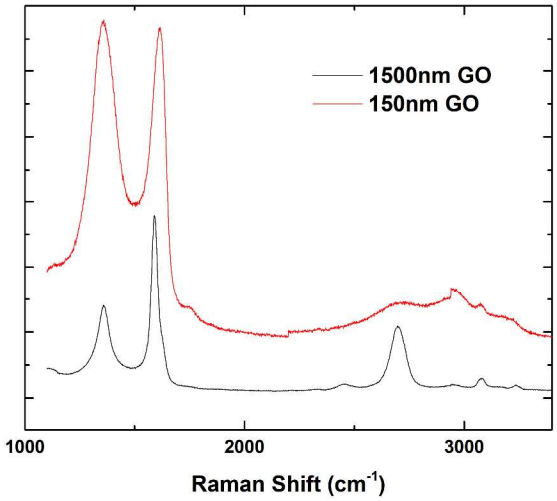

Figure S2. Raman spectroscopy of the two graphene oxide preparations used for cellular delivery studies. Spectra are vertically staggered for clarity. The approximate Raman shift of the D, G, 2D and D+G bands are 1350 cm^{-1}, 1584 cm^{-1}, 2700 cm^{-1}, and 2934 cm^{-1}, respectively.

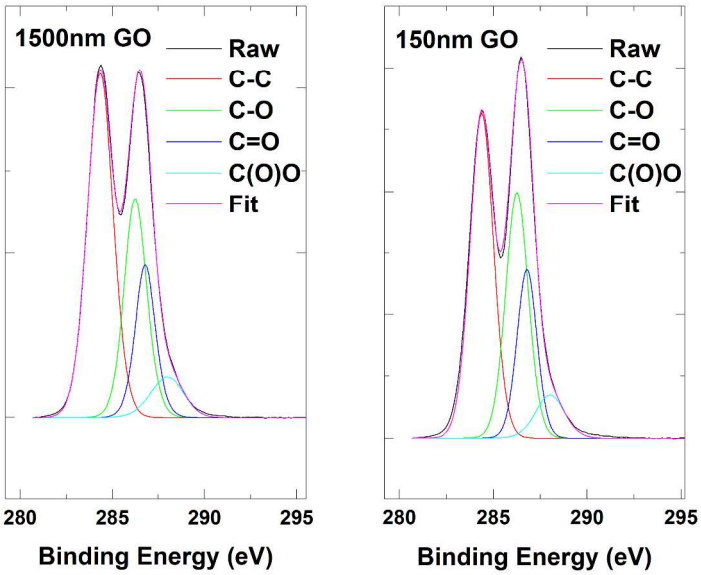

Figure S3. X-ray photoelectron spectroscopy of the two graphene oxide preparations used for cellular delivery studies. The 150 nm GO contains 10%-15% more oxygen groups compared to the 1500 nm GO.

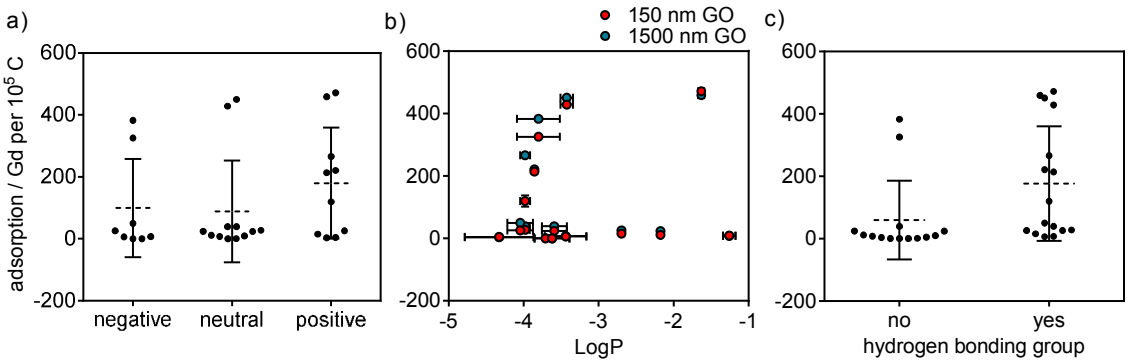

Figure S4. Adsorption as a function of a) charge, b) hydrophobicity, and c) hydrogen bonding potential of the adsorbing molecule on GO. No significant correlation was observed between adsorption and any of the chemical variables, indicating that GO adsorption in media cannot be simply predicted by charge interaction, hydrophobicity (for LogP < 0), or hydrogen bonding alone. Hydrophobicity was measured by the water-octanol partition coefficient. The hydrogen bonding groups include hydroxyl, phosphate, carboxylic acid, and primary amine. a) and c) combine data from the 150 nm and the 1500 nm GO. Dashed lines in a) and c) show mean. Error bars show SD in a) and c), and SEM in b).

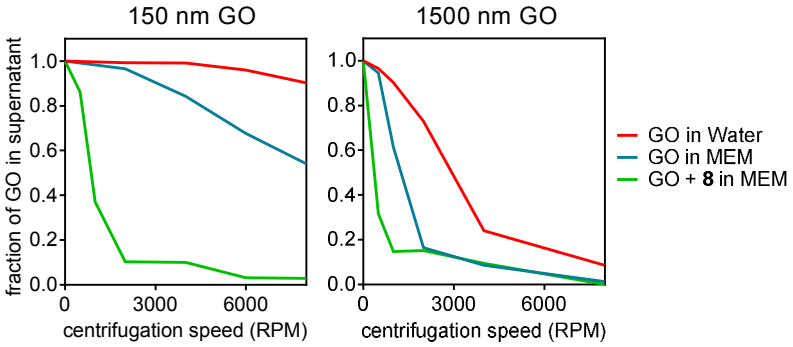

Figure S5. GO exhibits increased sedimentation in media supplemented with 10% FBS as compared to in water. Further increase in sedimentation can be observed when the GO surface interacts with a cargo molecule. The 1500 nm GO sediments more than the 150 nm GO.

2.2. Multiple Linear Regression Analysis

Multiple linear regression was used to construct a predictive model of the fold delivery enhancement achievable for small molecules when GO is used as a co-incubation vehicle. The result of regression found molecular adsorption, GO sedimentation, and GO size to be significant explanatory factors of delivery. Higher adsorption, faster sedimentation, and smaller GO size enhanced delivery. To ensure that this conclusion did not result from a violation of the assumptions of multiple linear regression, the r^2 change of adding and removing factors, and the p value and the variance inflation factor (VIF) of each explanatory variable were examined.

The r^2 examined were adjusted r^2 that take into account the spurious increase in r^2 when extra explanatory factors are added to a model. When the explanatory factors adsorption, size, and sedimentation were added in order into the model, the r^2 increased from 0.67 to 0.71 to 0.92. In the final 3-factor model, all of the factors had a p value < 10^{-6} and a VIF < 10. Multiple linear regression assumes a lack of collinearity among the explanatory factors, and a VIF below 10 confirms that the assumption has not been violated. Together, these results indicate that adsorption, sedimentation, and size all independently contribute to the predictive power of the final linear model.

For further validation, predictions made by the model can be confirmed qualitatively. First, adsorption was observed to increase delivery even for molecules that did not induce additional sedimentation (Figure S6). This result held true for both sizes of GO, confirming that adsorption correlates with delivery enhancement independent of sedimentation and size. Second, although **9** exhibited reduced adsorption compared to **12** (Figure 3a), it achieved a fold delivery enhancement that matched or even surpassed **12** upon GO co-incubation (Figure 3c). This result can be attributed to the increased GO sedimentation that **9** induced compared to **12**, confirming that sedimentation has power in explaining delivery enhancement independent of adsorption. Third, given the same level of sedimentation and adsorption (e.g. **11** + 150 nm GO and **11** + 1500 nm GO), the 150 nm GO outperformed the 1500 nm GO in delivery, confirming that size is an independent predictor of delivery enhancement. Thus, the 3-factor multiple linear regression model of GO delivery enhancement is validated both qualitatively and statistically.

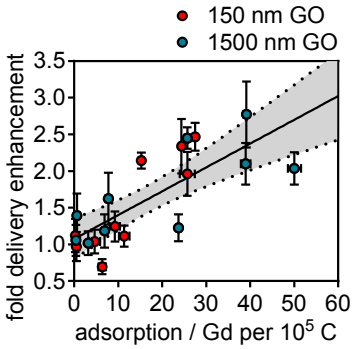

Figure S6. A significant correlation between delivery enhancement and adsorption can be found for molecules that did not increase GO sedimentation. The correlation was found for both the 150 nm and the 1500 nm GO. Adsorption predicts delivery enhancement independent of size and sedimentation. Error bars show SEM. Gray band shows 95% confidence interval.

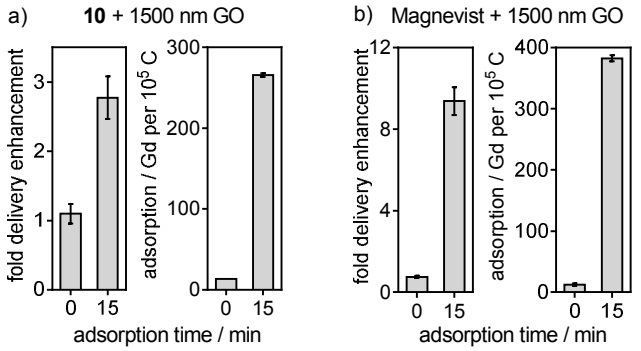

Figure S7. Additional adsorption time studies. Figure 5c showed that both molecular adsorption and delivery enhancement were abolished when a Magnevist-150 nm GO mixture was added directly to media without allowing for adsorption time. The same result was found with a mixture of a) **10** + 1500 nm GO and b) Magnevist + 1500 nm GO. Experiments were performed with 188 µM Gd(III) concentration and 18.8 µg/mL GO incubation concentration. Error bars show SEM.

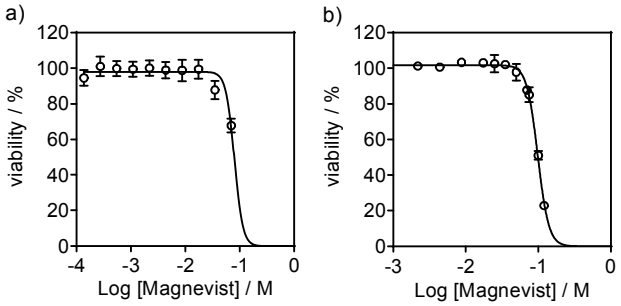

Figure S8. Cytotoxicity of Magnevist. a) Viability of HeLa cells at increasing Magnevist concentration as measured by the Guava ViaCount Assay. Analysis includes floating cells at the end of the 24-hr incubation period. The fitted IC50 was 80 mM. b) Same as in a) except analysis was performed after in-plate washing by PBS and does not include floating cells. The IC50 found was 99 mM, comparable to the result obtained in a). The Hill slope was found in b) and fixed in a) to keep the two fits comparable. Fitting was performed using GraphPad Prism software. All incubations were performed for 24 hours. Error bars show SD.

2.3. Robustness of GO Co-incubation Protocol

The robustness of the GO co-incubation protocol was evaluated in terms of 1) generalizability across cell lines, 2) inherent variability, and 3) sensitivity to procedural parameters.

Two molecular cargos, **10** and **12**, were co-incubated with GO on KB and HeLa cells to assess the effect of cell line on GO delivery. The result showed similar delivery enhancement by GO regardless of the cell line used (Figure S9), suggesting that GO co-incubation is indeed a delivery strategy that can be generalized beyond HeLa cells.

To characterize the inherent variability of the co-incubation protocol, the coefficient of variation (%CV) was used to measure data spread. %CV is defined as the ratio of the standard deviation to the mean. Beyond experimental error, inherent data spread arises due to complexities in cellular behavior, serum components, and nanomaterial synthesis. At 35 mM [Magnevist] and 20 μg/mL [GO], Magnevist uptake with and without GO resulted in 515 ± 319 (62% CV over 17 trials) and 115 ± 32 (28% CV over 10 trials) fmol Gd/cell, respectively (Figure S10). The increased variability observed with GO co-incubation may be attributed to varying degrees of GO sedimentation across multiple experiments. The Magnevist-GO combination would be particularly susceptible to this type of variability because it exhibited only moderate sedimentation in media (Figure 3b), making it possible for environmental factors such as cellular secretions or uncontrolled serum components to further induce sedimentation and change delivery. For variability in nanomaterial synthesis, a 23% CV in cell uptake was observed across three batches of GO (Figure S10). Overall, the inherent variability found is smaller than the average delivery enhancement achieved with GO co-incubation. Therefore, while the degree of enhancement can vary from experiment to experiment, GO can consistently be expected to increase cellular delivery.

To characterize procedural robustness, variations were made to the standard cellular assay that used 25,000 cells per well in a 24-well plate with in-plate washing. From this baseline, it was found that increasing the cell density to 75,000 cells per well, assaying in a 6-well plate, and adding a centrifugation wash step lowered the cellular Gd(III) content by 53%, 39%, and 71%, respectively (Figure S11). Similarly, using GO concentrations higher than 20 μg/mL resulted in a decrease in delivery, likely due to the formation of flocculants and aggregates that can interfere with cellular interaction and entry (Figure S11). These procedural parameters evidently play a significant role in the GO co-incubation protocol and should not be overlooked in future experimental design.

As an example, cells used for MRI had lower Gd(III) contents compared to those from other studies due to a change in labeling vessel and the centrifugation step needed to control cell density. At 35 mM [Magnevist] and 20 μg/mL [GO], the typical cellular Gd(III) content was 299 ± 67 fmol/cell with GO (N=11) and 91 ± 9 fmol/cell without GO (N=4) (3.3x enhancement) (Figure S10). In order to label a large number of cells for imaging, 6-well plates had to be used to replace the 24-well plates standard in the other studies. Moving from 24-well plates to 6-well plates decreased loading to 151 ± 56 fmol/cell with GO (N=13) and 49 ± 19 fmol/cell without GO (N=4) (3.1x enhancement). In order to control cell density for imaging, centrifugation was employed. The additional step resulted in the removal 60-70% of the Gd(III) labels, attributed to membrane binding (Figure S11). In the imaging study, the loading

achieved was 153 fmol/cell with GO and 69 fmol/cell without GO (2.2x enhancement) before centrifugation, and 47 fmol/cell with GO (69% label loss) and 30 fmol/cell without GO (57% label loss) after centrifugation.

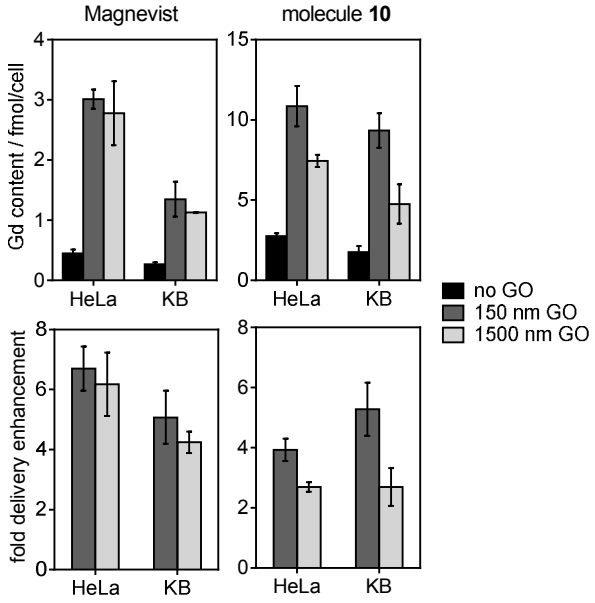

Figure S9. The generalizability of GO co-incubation as a strategy to enhance cellular delivery was demonstrated in the KB cell line. Similar levels of delivery enhancement were achieved in KB compared to HeLa. This result generalized across **10** and Magnevist (**12**) for both the 150 nm and the 1500 nm GO. Experiments were performed with 188 µM Gd(III) concentration and 18.8 µg/mL GO incubation concentration. Error bars show SD for Gd content and SEM for delivery enhancement.

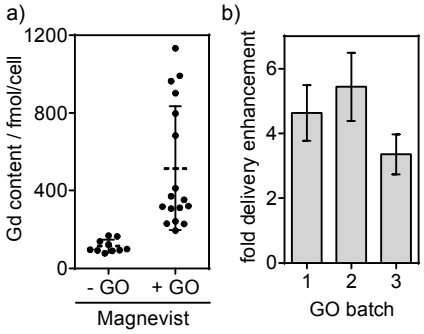

Figure S10. Inherent variability in cell delivery by GO co-incubation. a) Magnevist cell labeling with and without GO (150 nm) resulted in %CVs of 62% over 17 trials and 28% over 10 trials, respectively. b) A %CV of 23% was measured across 3 batches of 100-150 nm GO in the delivery of **10**. The intra-batch %CV averaged to 33%. Batch 3 was used for all other studies. Experiments in a) were performed with 35 mM Gd(III) concentration and 20 µg/mL GO incubation concentration. Experiments in b) were performed with 188 µM Gd(III) concentration and 18.8 µg/mL GO incubation concentration. Dashed lines in a) show mean. Error bars show SD in a) and SEM in b).

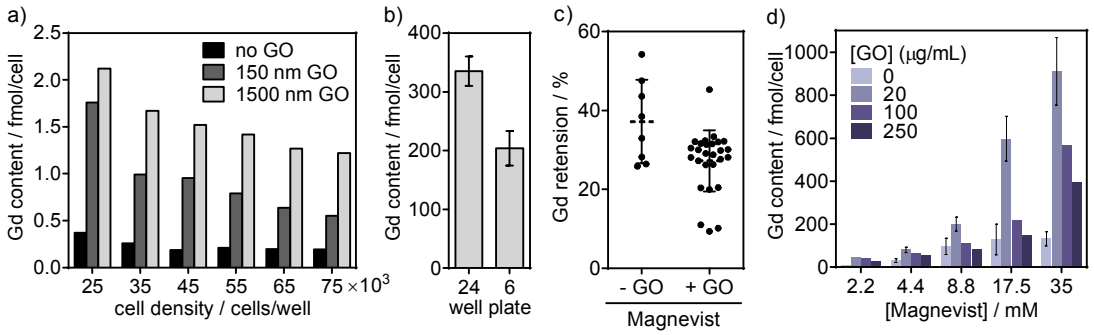

Figure S11. Sensitivity of the GO co-incubation protocol to procedural parameters. a) Cellular uptake of Magnevist with and without GO co-incubation decreases with cell density. b) Cellular Gd content decreases when incubating in a 6-well plate compared to a 24-well plate. c) 30%-40% of the cellular Gd content is retained upon washing by centrifugation. The portion washed away is attributed to membrane binding. d) Delivery enhancement achieved by GO (150 nm) co-incubation decreases above 20 μg/mL. Experiment in a) was performed in a 24-well plate at 188 μM Gd(III) concentration and 18.8 μg/mL GO concentration. Experiments in b) and c) were performed at 35 mM Gd(III) concentration and 20 μg/mL GO (150 nm) concentration. Error bars show SD.

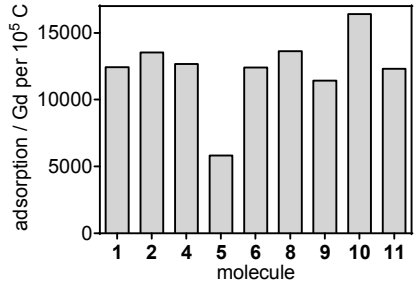

Figure S12. Adsorption as characterized by measuring the amount of Gd left in the supernatant after the GO has been centrifuged into a pellet. These numbers are 30-1000 times greater than those measured directly from the pellet after washing. Direct measurement of adsorption on the GO pellet is considered to be the more reliable method of the two. The 150 nm GO was used for this experiment.

3. Supplementary Tables

Table S1. GO Size Summary

	Square root of area (nm)		Height (nm)	
Sample	Mean	Median	Mean	Median
150 nm GO	179.3	144.3	0.86	0.84
1500 nm GO	1676.6	999.8	0.90	0.85

AFM data for the 150 nm GO is reported in Ref 7

Table S2. Chemical Characteristics of Gd(III)-labeled Small Molecules

Molecule	Charge	Hydration Number	Water-Octanol LogP	Hydrogen Bonding Group
1	0	1	-2.18 ± 0.02	
2	0	1	-3.98 ± 0.06	- OH
3	-1	1	-4.05 ± 0.17	- OPO_3H
4	+1	1	-2.69 ± 0.01	- NH_2
5	-1	1	-3.44 ± 0.28	- CO_2H
6	+1	1	-4.33 ± 0.46	
7	0	1	-1.26 ± 0.08	
8	0	2	-3.71 ± 0.02	
9	+1	2	-3.86 ± 0.01	- NH_2
10	+1	2	-3.98 ± 0.07	- NH_2
11	+1	2	-1.63 ± 0.04	- NH_2
12	-2	1	-3.80 ± 0.29	
13	0	1	-3.42 ± 0.08	- NH_2
14	0	1	-3.59 ± 0.16	
15	-1	1	-3.62 ± 0.23	

Errors show SD

Table S3. Delivery of Gd(III)-labeled Molecules With and Without GO

Molecule	Gd content (fmol/cell)											Outliers			
1	0.62	0.67	0.36	0.63	0.40										
+ 150 nm GO	0.63	0.63	0.44	0.58	0.57	0.76	0.57					1.11	1.24		
+ 1500 nm GO	0.59	0.58	0.39	0.77	0.86	0.76	0.64					1.18	1.45		
2	0.30	0.38	0.36												
+ 150 nm GO	0.84	0.81	0.90												
+ 1500 nm GO	0.59	0.88	0.70												
3	0.74	0.90	0.65												
+ 150 nm GO	1.84	1.36	1.29												
+ 1500 nm GO	1.61	1.64	1.41												
4	0.28	0.28	0.30	0.32	0.34										
+ 150 nm GO	0.73	0.62	0.61	0.65	0.64										
+ 1500 nm GO	0.63	0.80	0.73	0.74	0.82										
5	0.51	0.26	0.26	0.23	0.34	0.36						0.76			
+ 150 nm GO	0.31	0.25	0.13	0.16	0.17	0.20	0.23	0.29	0.22	0.23	0.33	0.66	0.76	0.62	
+ 1500 nm GO	0.58	0.27	0.33	0.30	0.31	0.53						1.00			
6	0.52	0.29	0.25	0.36	0.37										
+ 150 nm GO	0.37	0.29	0.42	0.43								2.73			
+ 1500 nm GO	0.42	0.36	0.32												
7	0.78	0.72	0.40	0.47	0.58										
+ 150 nm GO	1.13	0.53	0.68	0.73	0.47	0.87	0.73					3.26			
+ 1500 nm GO	1.29	1.24	0.67	0.64								4.12			
8	0.47	0.39	0.51	0.46	0.75	0.83						4.93*	4.31*		
+ 150 nm GO	0.53	0.39	0.39	0.42	0.44	0.44	1.09	0.73				13.51	3.25		
+ 1500 nm GO	0.63	0.55	0.68	0.50	1.05	1.36						6.54	4.00		
9	0.68	1.78	1.87	1.16	0.94	1.30	1.48								
+ 150 nm GO	13.40	20.22	14.84												
+ 1500 nm GO	7.61	7.56	6.31												
10	6.86	7.54	4.78	7.33	8.77	6.65	7.40					13.02*	14.46*	18.05	24.04
+ 150 nm GO	28.63	32.09	29.78												
+ 1500 nm GO	11.67	20.36	14.83												
11	3.88	5.08	4.54												
+ 150 nm GO	45.53	50.10	48.08												
+ 1500 nm GO	14.47	26.93	18.26												
12	0.34	0.30	0.54	0.82	0.51	0.72	0.61	0.61							
+ 150 nm GO	2.36	2.49	4.37	4.24	5.87	2.95	2.73	2.85							
+ 1500 nm GO	5.16	5.75	4.01	3.75	3.78	3.36									
13	1.99	3.84	1.83	1.26	1.04	1.29	2.63	2.80							
+ 150 nm GO	23.98	30.83	26.16												
+ 1500 nm GO	24.27	20.08	13.86	16.98	19.90										
14	0.51	0.42	0.61												
+ 150 nm GO	1.09	1.47	1.02												
+ 1500 nm GO	1.36	1.84	0.82	1.59	1.47							0.53*	0.55*		
15	0.22	0.31	0.20												
+ 150 nm GO	0.35	0.26	0.21												
+ 1500 nm GO	0.34	0.21	0.18	0.31								4.32			
150 nm GO	0.08	0.01													
1500 nm GO	-0.01	-0.01	-0.01												

Outliers were removed using Chauvenet's criterion unless marked. *removed based on experimenter judgment.

Table S4. Multiple Linear Regression Model Coefficients and Statistics

Predictor	Coefficient ± SEM	p value	VIF
Constant	11.3 ± 1.1		
Adsorption (Gd/10^5C)	$1.0 \pm 0.1 \times 10^{-2}$	1.6×10^{-7}	1.7
Sedimentation (AUC)	$-1.4 \pm 0.2 \times 10^{-3}$	4.6×10^{-9}	4.5
Size (nm)	$-7.2 \pm 0.8 \times 10^{-3}$	9.2×10^{-10}	3.7

Table S5. Experimental Replicate Numbers

Figure	N (range)	Average %CV
3a adsorption (Gd/10^5 C)	3.5 (3-5)	11%
3b sedimentation (AUC)	1.4 (1-2)	
3c Gd content (fmol/cell)	4.8 (3-11)	25%
5a Gd content (fmol/cell)	5.2 (4-6)	23%
5c adsorption time	3.7 (3-4)	

4. Supplementary References

1. Hong, V.; Presolski, S. I.; Ma, C.; Finn, M. G. Analysis and Optimization of Copper-Catalyzed Azide–Alkyne Cycloaddition for Bioconjugation. *Angew. Chem. Int. Ed.* **2009,** *48*, 9879-9883.
2. Chan, T. R.; Hilgraf, R.; Sharpless, K. B.; Fokin, V. V. Polytriazoles as Copper(I)-Stabilizing Ligands in Catalysis. *Org. Lett.* **2004,** *6*, 2853-2855.
3. Mastarone, D. J.; Harrison, V. S. R.; Eckermann, A. L.; Parigi, G.; Luchinat, C.; Meade, T. J. A Modular System for the Synthesis of Multiplexed Magnetic Resonance Probes. *J. Am. Chem. Soc.* **2011,** *133*, 5329-5337.
4. Axelsson, O.; Olsson, A. Synthesis of Cyclen Derivatives. WO/2006/112723, 2006.
5. Manus, L. M.; Mastarone, D. J.; Waters, E. A.; Zhang, X.-Q.; Schultz-Sikma, E. A.; MacRenaris, K. W.; Ho, D.; Meade, T. J. Gd (III)-Nanodiamond Conjugates for MRI Contrast Enhancement. *Nano Lett.* **2009,** *10*, 484-489.
6. Hung, A. H.; Duch, M. C.; Parigi, G.; Rotz, M. W.; Manus, L. M.; Mastarone, D. J.; Dam, K. T.; Gits, C. C.; MacRenaris, K. W.; Luchinat, C.*; et al.* Mechanisms of Gadographene-Mediated Proton Spin Relaxation. *J. Phys. Chem. C* **2013,** *117*, 16263-16273.
7. Chowdhury, I.; Duch, M. C.; Mansukhani, N. D.; Hersam, M. C.; Bouchard, D. Colloidal Properties and Stability of Graphene Oxide Nanomaterials in the Aquatic Environment. *Environ. Sci. Technol.* **2013,** *47*, 6288-6296.
8. Shen, Y.; Zhang, H.-B.; Zhang, H.; Ren, W.; Dasari, A.; Tang, G.-S.; Yu, Z.-Z. Structural Evolution of Functionalized Graphene Sheets During Solvothermal Reduction. *Carbon* **2013,** *56*, 132-138.
9. Abbas, A. N.; Liu, G.; Liu, B.; Zhang, L.; Liu, H.; Ohlberg, D.; Wu, W.; Zhou, C. Patterning, Characterization, and Chemical Sensing Applications of Graphene Nanoribbon Arrays Down to 5 nm Using Helium Ion Beam Lithography. *ACS Nano* **2014** 8 (2), 1538-1546.
10. Lerf, A.; He, H.; Forster, M.; Klinowski, J. Structure of Graphite Oxide Revisited. *J. Phys. Chem. B* **1998,** *102*, 4477-4482.
11. Gao, W.; Alemany, L. B.; Ci, L.; Ajayan, P. M. New Insights into the Structure and Reduction of Graphite Oxide. *Nat. Chem.* **2009,** *1*, 403-408.